Formation Spectra of the EPR Split Signals from the S_0, S_1, and S_3 States in Photosystem II Induced by Monochromatic Light at 5 K†

Ji-Hu Su,‡ Kajsa G. V. Havelius, Felix M. Ho, Guangye Han, Fikret Mamedov,* and Stenbjörn Styring*

Molecular Biomimetics, Department of Photochemistry and Molecular Science, Ångström Laboratory, Box 523, Uppsala University, SE-751 20 Uppsala, Sweden

Received March 1, 2007; Revised Manuscript Received June 1, 2007

ABSTRACT: The interaction EPR split signals from photosystem II (PSII) have been reported from the S_0, S_1, and S_3 states. The signals are induced by illumination at cryogenic temperatures and are proposed to reflect the magnetic interaction between $Y_Z^\bullet$ and the Mn_4Ca cluster. We have investigated the formation spectra of these split EPR signals induced in PSII enriched membranes at 5 K using monochromatic laser light from 400 to 900 nm. We found that the formation spectra of the split S_0, split S_1, and split S_3 EPR signals were quite similar, but not identical, between 400 and 690 nm, with maximum formation at 550 nm. The major deviations were found between 440 and 480 nm and between 580 and 680 nm. In the regions around 460 and 680 nm the amplitudes of the formation spectra were 25−50% of that at 550 nm. A similar formation spectrum was found for the S_2-state multiline EPR signal induced at 0 °C. In general, the formation spectra of these signals in the visible region resemble the reciprocal of the absorption spectra of our PSII membranes. This reflects the high chlorophyll concentration necessary for the EPR measurements which mask the spectral properties of other absorbing species. No split signal formation was found by the application of infrared laser illumination between 730 and 900 nm from PSII in the S_0 and S_1 states. However, when such illumination was applied to PSII membranes poised in the S_3 state, formation of the split S_3 EPR signal was observed with maximum formation at 740 nm. The quantum yield was much less than in the visible region, but the application of intensive illumination at 830 nm resulted in accumulation of the signal to an amplitude comparable to that obtained with illumination with visible light. The split S_3 EPR signal induced by NIR light was much more stable at 5 K (no observable decay within 60 min) than the split S_3 signal induced by visible light (50% of the signal decayed within 30 min). The split S_3 signals induced by each of these light regimes showed the same EPR spectral features and microwave power saturation properties, indicating that illumination of PSII in the S_3 state by visible light or by NIR light produces a similar configuration of $Y_Z^\bullet$ and the Mn_4Ca cluster.

Photosystem II (PSII)[1] is a multisubunit protein−cofactor complex in higher plants, green algae, and cyanobacteria (*1*, *2*). It catalyzes the photoinduced oxidation of water and reduction of the plastoquinone pool, thus initiating the electron transport chain of the thylakoid membrane. The water oxidation process occurs at the donor side of PSII at a catalytic site, composed of the Mn_4Ca cluster and a nearby redox-active tyrosine, Y_Z. In order to split water, the Mn_4Ca cluster cycles through five intermediate states denoted $S_0 \rightarrow S_4$, where the S_0 state is the most reduced state while the S_1 state is the dominating state in the dark (*3*). The S_2 and the S_3 states are metastable, oxidized states that decay to the S_1 state within a few minutes at room temperature. The S_4 state is a transient state that is formed during the $S_3 \rightarrow (S_4) \rightarrow S_0$ transition, concomitantly with the release of molecular oxygen from the Mn_4Ca cluster (*4*, *5*). In the meantime, the protons derived from water oxidation are released into the thylakoid lumen (*6*−*8*).

The redox properties of Y_Z are important for stable charge separation and the deprotonation reactions on the donor side of PSII (*6*−*8*). The direct observation of $Y_Z^\bullet$ in intact PSII by EPR spectroscopy is rather difficult due to its fast reduction by the Mn_4Ca cluster (*9*, *10*) and the fact that its EPR spectrum overlaps with the very similar spectrum from the stable oxidized radical Y_D. However, the short distance between the Mn_4Ca cluster and Y_Z (5−6 Å (*11*−*15*)) provides an advantage in this respect because, upon formation, the neutral $Y_Z^\bullet$ radical magnetically couples to the Mn_4Ca cluster giving rise to a split EPR signal. Such split EPR signals were first reported from PSII with a partially

† The financial support from the Knut and Alice Wallenberg Foundation, the Swedish Research Council, the Swedish Energy Agency, SOLAR-H (EU Network Program NEST 516510), and the European Community Sixth Framework Program, Marie Curie Incoming International Fellowship (514817 to F.M.H.), is gratefully acknowledged.

* Corresponding authors. Fax: +46 18 471 6844. Tel: +46 18 471 6580; +46 18 471 6581. E-mail: stenbjorn.styring@fotomol.uu.se; fikret.mamedov@fotomol.uu.se.

‡ Current address: Max Planck Institute for Bioinorganic Chemistry, Stiftstrasse 34-36, D-45470 Mülheim an der Ruhr, Germany.

[1] Abbreviations: Car, carotenoid; Chl, chlorophyll; DAD, 3,6-diamino-durol; DMSO, dimethylsulfoxide; ENDOR, electron−nuclear double resonance; EPR, electron paramagnetic resonance; EXAFS, extended X-ray absorption fine structure; MES, 2-(*N*-morpholino)-ethanesulfonic acid; NIR, near infrared; P_{680}, the primary electron donor in PSII; P_PBQ, phenyl-*p*-benzoquinone; PSII, photosystem II; Q_A and Q_B, the primary and secondary quinone acceptors in PSII; Y_D and Y_Z, the redox active tyrosine residues in PSII; WOC, water oxidizing complex.

10.1021/bi7004174 CCC: $37.00
Published on Web 08/24/2007

inhibited donor side (see a brief review in Petrouleas et al. 2005 (*16*) and in Havelius et al. 2006 (*17*) and references therein). Pulse ENDOR measurements in Ca depleted and acetate inhibited PSII membranes provided strong evidence that these split signals originate from magnetic coupling between $Y_Z^{\bullet}$ and the Mn_4Ca cluster (*18*, *19*).

Split EPR signals with quite similar EPR properties have also been reported to be induced in intact PSII centers by illumination at liquid He temperatures. Under these conditions, oxidation of Y_Z remains functional while the reduction of $Y_Z^{\bullet}$ by the Mn_4Ca cluster is blocked. Such split EPR signals were reported in the S_0, S_1, and S_3 states of PSII (*17*, *20*−*26*) and more recently in the S_2 state (*27*). The EPR spectra of the split S_1 and split S_3 signals are asymmetric: the former has a characteristic peak located at the low-field side of $g \sim 2.0$, and the latter has a characteristic double trough at the high-field side of $g \sim 2.0$ as well as a broad peak at the low-field side. The split S_0 and split S_2 signals resemble the split signals in inhibited PSII and are more symmetric and consist of a low-field peak and a high-field trough located around the $g \sim 2.0$ region (*17*, *20*−*25*, *28*).

The split signals were reported to be induced also from the S_2 and S_3 states by NIR illumination at 4 K or 50 K (*26*, *29*−*34*). This is particularly interesting since the effects of NIR light on the Mn_4Ca cluster are thought to reflect photochemistry within the cluster itself, probably by excitation of a Mn^{3+} ion (*16*, *26*, *29*, *32*, *35*−*37*). Thus, the different split EPR signals can be induced by different light qualities at the low temperatures.

In the present study, PSII samples poised in the different S states were illuminated with monochromatic laser flashes at 5 K to investigate the formation of the split S_0, split S_1, and split S_3 signals in the visible (415−690 nm) and in the NIR range (730−900 nm). Our results show that all three split signals were similarly induced by visible light. In addition, the split S_3 signal was also induced by NIR illumination at 5 K. The induction, stability, and relaxation properties of the split S_3 signal induced by visible or NIR illumination are also compared.

MATERIALS AND METHODS

PSII Membrane Preparation. PSII enriched membranes (BBY type) were prepared from hydroponically grown greenhouse spinach (*Spinacia oleracea*) according to refs *38* and *39*, resuspended in a buffer containing 400 mM sucrose, 25 mM MES−NaOH (pH 6.1), 15 mM NaCl, and 3 mM $MgCl_2$, and then stored at −80 °C before use. The oxygen evolution rate was 400−450 μmol of O_2 (mg Chl)$^{-1}$ h^{-1} when measured in the presence of 1.0 mM PpBQ as an electron acceptor with a Clarke type electrode. In order to avoid the strong absorption from the $Y_D^{\bullet}$ radical in the $g \sim 2.0$ region during EPR experiments, Y_D was reduced by an ascorbate (10 mM) and DAD (3 mM) treatment to 1−5% of its maximum size without altering the oxygen evolving activity, as described in refs *17* and *40*. The Chl concentration was determined as in ref *41*.

EPR Sample Preparation and EPR Measurements. After the addition of PpBQ (1 mM, dissolved in DMSO, 2% v/v), the samples (about 170 μL, ∼3 mg Chl/mL) were transferred to calibrated EPR tubes and incubated at 0 °C for 5−10 min. Then the samples were illuminated with 0, 1, 2, or 3 laser flashes from a Nd:YAG laser (5 Hz, 6 ns, 532 nm, pulse bandwidth ± <0.01 nm, 440 mJ/pulse) to predominantly induce the S_1, S_2, S_3, or S_0 states, respectively. When Y_D is reduced, the flash induced turnover of the S states is rapidly desynchronized as was observed previously due to misses and back reactions involving reduced Y_D (*17*, *24*, *43*). Moreover, we could not apply a synchronizing preflash treatment.[2] A two-flash sample, prepared with this reduction and flash protocol, was dominated by the S_3 state, although it also contained a considerable fraction of the centers in the S_2 state. The sample given three flashes was estimated to contain ∼50% of PSII in the S_0 state and ∼40% in the S_3 state as judged from the oscillation of S_2-state multiline signal, which is normal for this type of sample (*17*, *24*). After flashing, the samples were frozen within 1−2 s in a dry ice/ethanol bath and then rapidly transferred to liquid nitrogen. All steps were performed under dim green light.

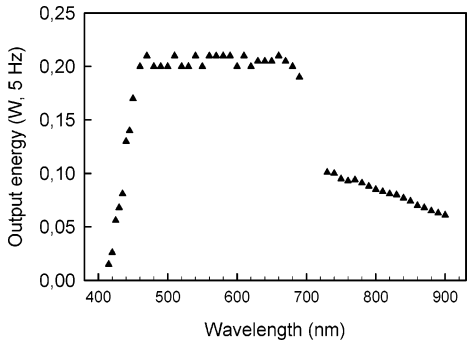

FIGURE 1: Wavelength dependence of the energy output from the MOPO. The energy provided by flashing at 5 Hz was measured at the position of the EPR sample. Due to instrument limitations, no laser light is obtainable between ca. 690 and 730 nm with our MOPO.

To investigate the formation spectra of the S_2-state EPR multiline signal at different wavelengths, the same pretreatment protocol was used except that the dark adapted samples were given one flash at 0 °C (6 ns, 415−690 nm, pulse bandwidth is ±0.1 nm) from the Quanta-Ray MOPO-730 optical parametric oscillator. For induction of the split signals at different wavelengths at 5 K, a train of laser flashes from the MOPO, provided between 415 and 690 nm and between 730 and 900 nm, were directed into the Bruker ST4102 standard or SHQ4122 high Q cavity. The energy of the laser flash from the MOPO was wavelength dependent and is shown in Figure 1 (measured with Scientech 372 power and energy meter, Scientech Inc., USA). When indicated, the split signals were sometimes induced by continuous illumination either using broadband white light from a 800 W projector lamp passed through 4 cm of $CuSO_4$ solution or using 830 nm light (from a LQC830-135E laser diode, Newport, USA, 135 mW output power at 830 nm) directed into the EPR cavity. The light intensities applied at the level for the EPR sample were 160 W/m^2 in the white light and 280 W/m^2 at 830 nm.

Low-temperature EPR spectra were recorded with a Bruker ELEXYS E500 spectrometer equipped with an Oxford-900

[2] Note that the preflash procedure often applied to synchronize the OEC to the S_1 state prior to the "actinic" flashes (*17*, *24*, *42*) could not be applied due to the preferred presence of Y_D in its reduced form. Had a preflash been used, Y_D would have been reoxidized in the majority of the centers.

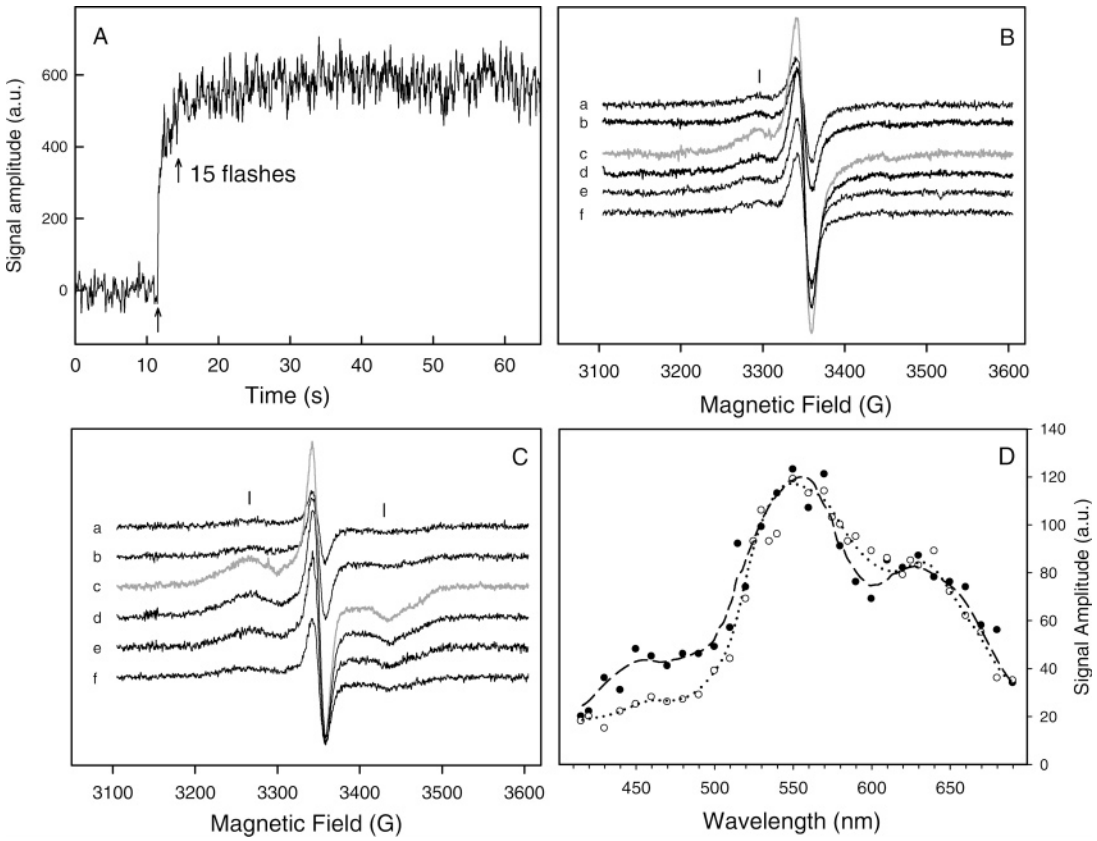

FIGURE 2: (A) Induction of the split S_1 signal by a train of laser flashes provided over ~50 s (5 Hz) at 530 nm at 5 K. The first arrow shows where the first laser flash was given, and the second arrow shows where 15 flashes had been given. The field position (at 3295 G) where the induction trace was recorded is indicated by the bar in panel B. (B, C) The difference EPR spectra (spectrum recorded after first 15 flashes at 5 Hz minus the spectrum recorded before flashing) of the split S_1 (B) and split S_0 (C) EPR signals induced by 15 laser flashes from the MOPO at (a) 450 nm, (b) 500 nm, (c) 550 nm, (d) 600 nm, (e) 650 nm, and (f) 680 nm. The bars indicate the field positions used for signal quantification. EPR settings: microwave frequency 9.41 GHz, microwave power 25 mW, modulation amplitude 10 G, illumination and measurement temperature 5 K. (D) Dependence of the signal amplitude at 3295 G (from the split S_1 signal in panel B (●), dashed line) and 3270 G (from the split S_0 signal in panel C (○), dotted line) on the wavelength of the applied flashes.

cryostat and ITC-503 temperature controller (Oxford Instruments Ltd.). The experimental settings are given in the figure legends. All data were analyzed with the Bruker Xepr 2.1 software.

RESULTS

In earlier studies, the split S_1, split S_3, and split S_0 EPR signals were assigned to the corresponding S states of the WOC (*17*, *28*). In the present paper, we have investigated how these signals are induced at 5 K as a function of the wavelength of the applied light in the visible and NIR region. To ensure the quality of the applied light we have induced the EPR signals using monochromatic light from a tunable flash laser.

The Formation Spectra of the Split S_1 and Split S_0 EPR Signals. It is known that both the split S_1 and split S_0 signals are inducible by visible light illumination (i.e., laser flashes at 532 nm) and do not require NIR light for their formation (*21*). The induction by flashes at 530 nm of the split S_1 signal recorded at 3295 G is shown in Figure 2A. The signal was quickly induced, and 70−80% of the maximum amplitude was reached after 3 s of flashing at 5 Hz. Very similar induction was observed by the application of laser flashes between 415 and 690 nm not only for the split S_1 signal but also for the split S_3 and split S_0 signals (data not shown). Therefore, 15 laser flashes were chosen to investigate the formation spectra of the split signals at 5 K in the visible region. Two sets of EPR spectra, induced by 15 monochromatic laser flashes between 415 and 690 nm, are displayed in Figures 2B and C. The EPR spectra show the characteristic features of the split S_1 and split S_0 signals in unflashed samples (i.e., mostly in the S_1 state) and samples provided 3 flashes at 0 °C (where the S_0 state dominated). All induced split S_1 signals displayed a peak located at ~3295 G on the low-field side of $g \sim 2.0$ (marked by a bar in Figure 2B), similar to the split S_1 spectra described earlier which were induced by broadband white light (*17*, *20*, *21*). All spectra also showed an unresolved peak around $g = 2$. The maximal signal induction after application of 15 laser flashes was achieved at 550 nm (Figure 2B, spectrum c, and Figure 2D, filled circles).

The overall shape of the EPR spectra of the split S_0 signal induced at different wavelengths (Figure 2C) was similar to the split S_0 signal described earlier (*17*, *21*). The spectra were symmetric, containing a peak centered at ~3270 G and a trough centered ~3450 G, located on either side of the peak at $g \sim 2.0$ (indicated by bars in Figure 2C). The maximal induction of the split S_0 signal was also achieved with flashes at 550 nm (Figure 2C, spectrum c, and Figure 2D, open circles).

The formation spectra for both signals are shown in Figure 2D. The split S_1 signal amplitude (measured at 3295 G) and

the split S_0 signal amplitude (measured at 3270 G) showed quite similar wavelength dependence over the 415−690 nm range (Figure 2D). The spectra are dominated by a maximal peak at ~550 nm, a shoulder at 630 nm, and lower signal yields in the regions of $\lambda \leq 500$ nm and $\lambda \geq 650$ nm. The formation spectra (normalized at 550 nm) vary somewhat between 430 and 500 nm where the split S_1 signal was more efficiently induced and between 575 and 620 nm where the split S_0 was more efficiently induced.

It is important that we were not able to form either the split S_1 or split S_0 signals at wavelengths above 730 nm, despite the application of up to 1500 laser flashes (data not shown).

Dependence of the Split Signal Formation on the Sample Chl Concentration. The similarity of the formation spectra for the split S_1 and split S_0 signals prompted us to study the concentration dependence of the split signal formation in order to reduce possible Chl interference. This was performed for the split S_1 signal since the S_1 state dominates in the dark adapted samples and does not require additional flashing procedures. The results are shown in Figure 3. We were certainly able to observe the formation of the split S_1 EPR signal after flash illumination of the samples at Chl concentrations above 1.5 mg/mL, but in the sample with a concentration below 1 mg/mL the signal was very small (Figure 3A). Despite the very small signals at low sample concentrations, it is clear that the signal amplitude increased linearly with the sample concentration in the concentration range studied (Figure 3B). We were not able to observe any wavelength-dependent deviation from linearity (Figure 3B) between 480 and 680 nm.

Five wavelengths were chosen to investigate the possible concentration dependence of the formation spectra (Figure 3C). At the Chl concentration of 2.8 mg/mL the formation spectrum was similar to that shown in Figure 2D. The peak around 550 nm and the shoulder around 630 nm were clearly visible (Figure 3C). As the concentration of the sample was decreased, the formation spectrum became more featureless with one overall broad peak between 550 and 600 nm reflecting the smaller EPR signal giving rise to a less resolved spectrum. At a concentration of 0.8 mg of Chl/mL the very small split signal (Figure 3A, spectrum d) was almost lacking any spectral information (Figure 3C).

The Formation Spectra of the S_2-State Multiline Signal at 0 °C. The formation of the split S_1 and split S_0 signals takes place after illumination of PSII at 5 K, where turnover of the WOC does not occur (*42*). Therefore, it was interesting to also study the wavelength dependence of induction of an EPR signal that involves oxidation of the Mn_4Ca cluster. The S_2-state multiline EPR signal is a well-studied probe of the $S_1 \rightarrow S_2$ transition that can be formed by a single flash applied to dark adapted PSII membranes. Here we studied the induction of this signal at 0 °C by single monochromatic light flashes between 415 and 690 nm. A series of the resulting spectra are partially shown in Figure 4A. The signal amplitude varies with the wavelength of the applied laser flash, and the signal reaches the largest amplitude between 530 (spectrum b) and 580 nm (spectrum c). In addition, it is clear that the shape of the EPR spectrum was not dependent on the applied flash wavelength. The spectra in Figure 4A only show the low-field part of the multiline signal, but the same conclusions hold also for the

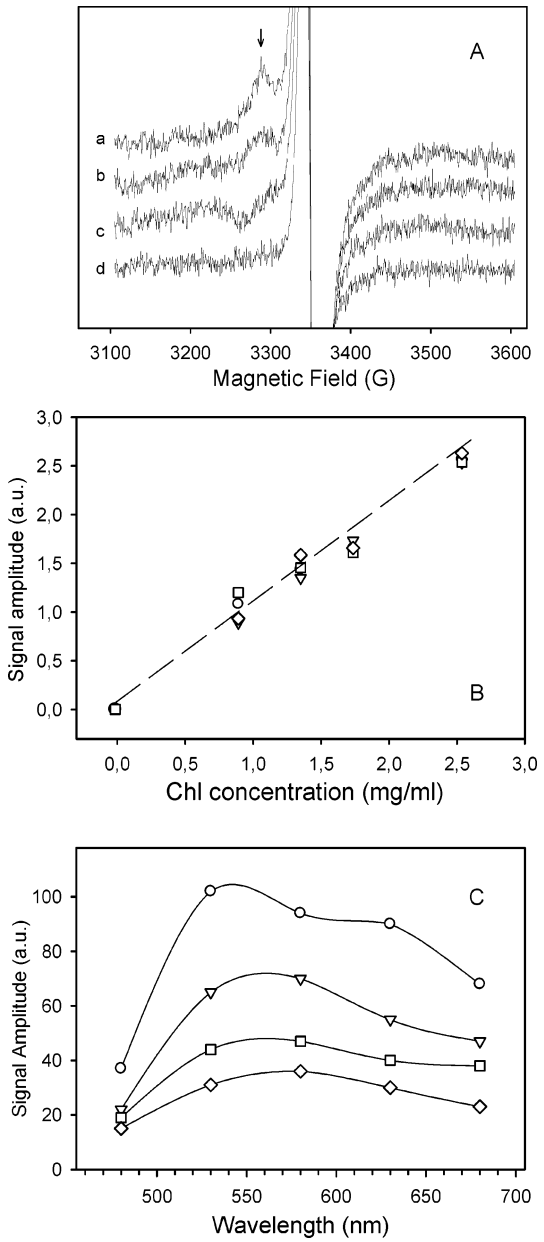

FIGURE 3: (A) The difference EPR spectra (spectrum recorded after first 100 flashes at 5 Hz minus the spectrum recorded before flashing) of the split S_1 EPR signal induced by laser flashes from the MOPO at 530 nm in the PSII membrane samples at a Chl concentration of (a) 2.80 mg/mL, (b) 2.21 mg/mL, (c) 1.56 mg/mL, and (d) 0.79 mg/mL. (B) Dependence of the normalized split S_1 EPR signal intensity measured at 3295 G (position indicated by the arrow in Figure 3A) on the sample Chl concentration. The split S_1 EPR signal was induced by100 flashes at (▽) 480 nm, (○) 530 nm, (□) 630 nm, and (◇) 680 nm. (C) Formation spectra of the split S_1 EPR signal induced by 100 laser flashes from the MOPO in PSII samples at a Chl concentration of (○) 2.80 mg/mL, (□) 2.21 mg/mL, (▽) 1.56 mg/mL, and (◇) 0.79 mg/mL.

spectra at the high-field side of $g = 2.0$ (data not shown). The amplitude of the S_2-state multiline signal induced by the relatively weak laser flash from the MOPO (40 mJ) at 540 and 480 nm was 60% and less than 20% respectively of the maximally inducible signal using a saturating laser flash at 532 nm (440 mJ) followed by illumination at 200 K (not shown).

The formation spectrum of the S_2-state multiline EPR signal is shown in Figure 4B. It has maximal induction at

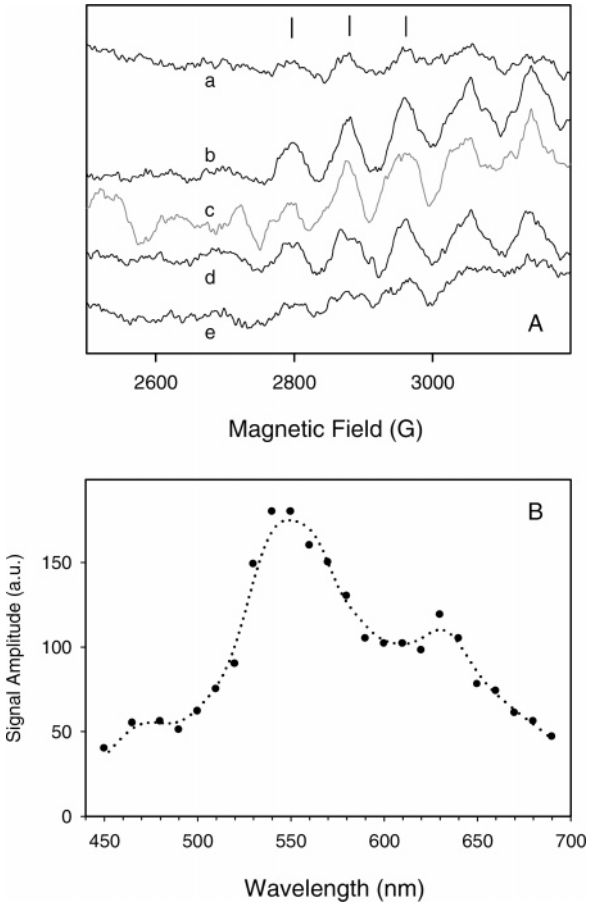

FIGURE 4: (A) EPR spectra displaying part of the S_2-state multiline signal in the $g > 2.0$ region of the signal induced by a single monochromatic laser flash at 0 °C. The signals were induced at (a) 480 nm, (b) 530 nm, (c) 580 nm, (d) 630 nm, and (e) 680 nm. The bars indicate the field positions used for signal quantification. EPR settings: microwave frequency 9.41GHz, microwave power 25 mW, modulation amplitude 15 G, temperature 7 K. (B) Dependence of the S_2-state multiline EPR signal amplitude on the wavelength of the applied laser flash.

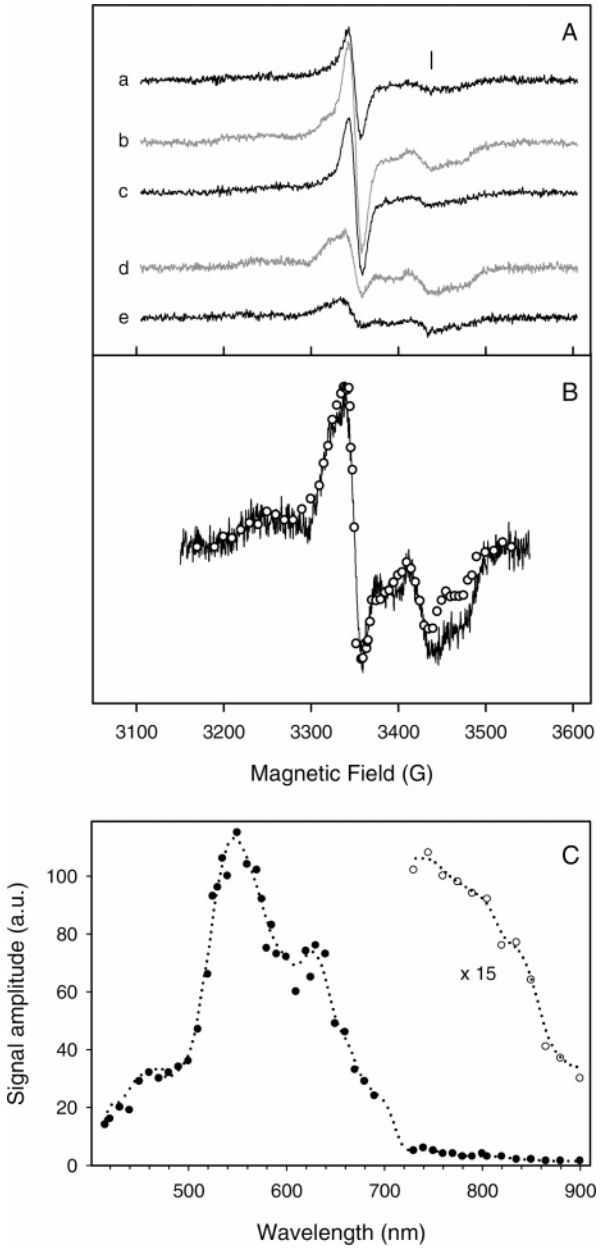

FIGURE 5: (**A**) Light minus dark difference EPR spectra of the split S_3 EPR signal induced by laser flashes at (a) 450 nm, (b) 550 nm, (c) 650 nm, (d) 750 nm, and (e) 850 nm. Spectra in the visible range (a−c) were induced by 15 flashes, and spectra in the NIR region (d, e) were induced by 1500 flashes given at 5 K and at 5 Hz repetition rate. The bar indicates the field position used for signal quantification. EPR settings as in Figure 2. (B) Comparison of a split S_3 spectrum induced by NIR illumination (the same as spectrum d from panel A, line) and the decay-associated spectrum induced by visible light (split S_3 signal with $t_{1/2} \sim 3$ min from ref *17*, open circles). (C) Dependence of the signal amplitude of the split S_3 signal on the wavelength of the applied flashes in the visible and NIR region.

∼540 nm (Figure 4B) with a shoulder at 630 nm, and low yield in the regions of $\lambda \leq 500$ nm and $\lambda \geq 650$ nm. Most of the spectral features are similar to those of the split S_1 and split S_0 signals (Figure 2D).

In addition, we note that no induction of the S_2-state multiline EPR signal was observed after application of a single flash in the NIR region (not shown).

The Formation Spectrum of the Split S_3 Signal. The split S_3 signal was induced by providing monochromatic laser flashes at 5 K to samples which were dominated by PSII centers in the S_3 state (i.e., samples provided with 2 flashes at 0 °C). Figure 5A displays a set of EPR spectra of the split S_3 signals obtained by 15 flashes at (a) 450 nm, (b) 550 nm, and (c) 650 nm light in the visible region. All these spectra have similar features: a trough centered around 3440 G on the high-field side of $g \sim 2.0$ and a weaker peak around 3220−3260 G. These spectral characteristics are similar to those reported in our previous papers where the signal was induced by white light (*17*, *28*, *44*). In addition, the signal amplitude induced by flashes at 550 nm was higher than those obtained by induction at 450 and 650 nm. It is important to note that visible light illumination used here also resulted in the formation of a peak around $g \sim 2.0$. This peak was analyzed before and demonstrated to contain a mixture of a feature from the split S_3 signal itself and a nondecaying radical species assigned to an oxidized Car (*17*).

We also studied the induction at 5 K of the split S_3 signal by light >730 nm but were not able to observe any clear signals after 15 laser flashes in the NIR region. However, when the number of applied flashes was significantly increased, the signal from the S_3 state could be detected. Spectra d and e in Figure 5A are light minus dark difference spectra after the application of 1500 flashes at 750 and 850

nm, respectively. It is immediately clear that these spectra are remarkably similar to the split S_3 spectra induced by visible illumination (spectra a−c) in the wings of the EPR spectrum. They contain the same characteristic troughs located around 3440 G (marked by the bar in Figure 5A) and a broad weak peak around 3220−3260 G. Thus, illumination by NIR light resulted in the formation of the split S_3 signal but at very low quantum yield when compared to induction by visible light flashes between 415 and 690 nm.

An interesting observation is that the spectra obtained by flashes at 750 and 850 nm (Figure 5A, spectra d and e) differ from the spectra obtained by visible light (Figure 4A, spectra a−c) in the middle part of the EPR spectrum (3340−3360 G). Our earlier analysis of the decay associated spectra of the split S_3 signal induced by visible illumination (*17*) revealed that the EPR peak around $g = 2.0$ contained a broader part from the split S_3 signal and a ca. 10 G wide radical signal. The radical signal was assigned to a Car radical. Interestingly, flash illumination by the NIR light resulted in EPR spectra (Figure 5A, spectra d and e) which are devoid of the narrow peak from the Car radical. The spectrum is almost identical to that of the kinetically deconvoluted split S_3 signal (Figure 5B (*17*)). Thus, the NIR illumination did not result in oxidation of the Car auxiliary donor even though the species involved in the split S_3 signal were still formed.

The plot in Figure 5C shows the formation spectrum of the split S_3 signal. In the visible light range it was essentially the same as the formation spectra of the split S_1, the split S_0, and the S_2-state multiline signals, with maximal formation at 540 nm and a shoulder at 630 nm. By contrast, it is clear that the application of laser flashes above 730 nm resulted in the formation of the split S_3 EPR signal. The formation seems to be most efficient at 740 nm and declines at higher wavelengths. It is however also clear that we observe induction of the split S_3 signal in the entire investigated NIR spectral region between 730 and 900 nm (Figure 5C).

Comparison of the Split S_3 Signals Induced by Visible and NIR Light. An important question is whether there are differences in the EPR spectral properties of the split S_3 signal induced by visible ($415 \leq \lambda \leq 690$ nm, Figure 5A, spectra a−c) and by NIR ($\lambda \geq 730$ nm, Figure 5A, spectra d and e) irradiation. We address this in the following section.

Decay Kinetics of the EPR Spectrum. As mentioned before, the split S_3 signal induced by NIR illumination (Figure 5B, line spectrum) is remarkably similar to the deconvoluted, decay associated split S_3 spectrum induced by visible light (Figure 5B, open circle spectrum, see ref *17* for details). In the latter spectrum the $g \sim 2$ radical spectrum assigned to a Car^+ radical had been removed by kinetic analysis while this component never was formed in the split S_3 spectrum induced by NIR illumination. We thus conclude that these spectra (Figure 5B) represent clean, uncontaminated spectra of the split S_3 signal recorded under illumination with either visible or NIR light.

To investigate the stability of the split S_3 EPR signal induced by visible and NIR irradiation, PSII samples in the S_3 state were illuminated for prolonged times at 5 K by broadband white light or strong NIR light at 830 nm provided from a laser diode. Thereafter the decay kinetics at 5 K in the dark were followed as in ref *17*. The results are displayed in Figure 6A, where the amplitude of the split S_3 signal at 3440 G (marked by the bar in Figures 5A and 6B) is plotted as a function of time. When induced by visible light, the signal kinetics (Figure 6A, filled circles) could be differentiated into one decaying (52%) and one stable (48%) component. By contrast, the signal induced by NIR irradiation was composed of a single stable part which did not decay even after 60 min dark incubation at our measuring temperature (5 K, Figure 6A, open circles).

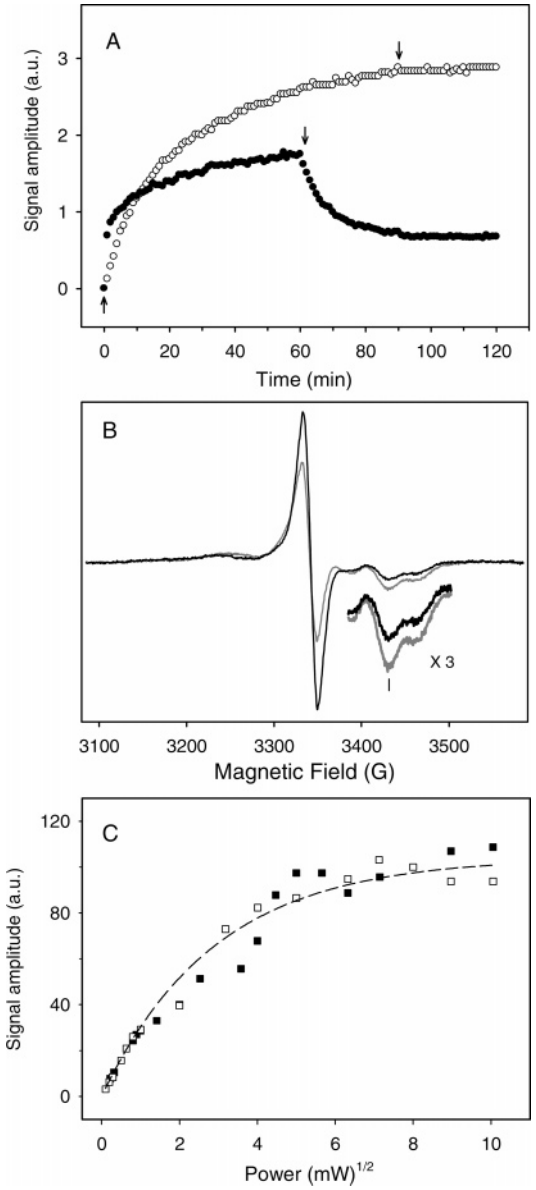

FIGURE 6: (A) Induction and decay of the split S_3 EPR signal followed at 3440 G (see bar in Figures 5A and 6B) when the signal was induced by continuous broadband white light (see Materials and Methods) (●) and by continuous illumination at 830 nm from a laser diode (○). The formation and decay kinetics were followed by recording a new spectrum every 60 s. (B) Light minus dark difference EPR spectra of the split S_3 EPR signal induced by continuous illumination by white light (black) or 830 nm light (gray). Amplification of the signal at high field trough is shown for better comparison. The spectra are recorded at the end of the illumination phase in panel A. EPR settings as in Figure 2 except that the microwave frequency is 9.37 GHz. (C) Microwave power saturation of the split S_3 signal induced by visible light at 560 nm (15 flashes (■)) and by NIR light at 800 nm (1500 flashes (□)). EPR settings as in Figure 2. The signal amplitude was measured at 3440 G (see bar in Figure 4A).

Illumination with 1500 flashes in the NIR resulted only in a fraction of the signal amplitude induced by visible light (Figure 5C) seemingly implying that it was not possible to induce the split S_3 signal in all PSII centers with the NIR illumination. This was tested in the experiment shown in Figure 6A, where much more extensive illumination was applied over longer time both in the visible and in the NIR. Interestingly, illumination with broad white light for as much as 60 min did not increase the signal yield as compared to the signal amplitude obtained with the flashing light. By contrast, extensive illumination with a continuous 830 nm laser diode resulted in a much increased amplitude of the signal compared to the amplitude reached by our MOPO flash laser. The maximal amplitude was almost 35% higher amplitude than obtained with the visible light (Figure 6A). This indicates that, although less efficient, photoaccumulation with NIR light can produce the species giving rise to the split S_3 signal in even more centers than visible light.

It is also useful that the strong illumination with the NIR laser diode resulted in a "clean" split S_3 signal comparable to the signal shown in Figure 5B. This is shown in Figure 6B where EPR spectra recorded close to the end of the prolonged illumination in the visible or at 830 nm displayed in Figure 5A are shown. The two spectra differ both in amplitude and in shape. From the amplitudes in the wings of the spectra, it is clear that the illumination at 830 nm induced a larger split S_3 signal than the extensive illumination with the visible light. In addition, the spectral shapes are different and the middle part (the $g \sim 2.0$ region) of the spectrum induced with visible light is larger in amplitude than the corresponding part in the NIR induced spectrum. As described before (*17*), this reflects the induction of a Car radical by the visible light, which is not formed by the illumination at 830 nm.

Microwave Power Saturation. The microwave power saturation at 5 K of the split S_3 signal induced either by visible or by NIR irradiation was also investigated (Figure 6C). Both signals displayed similar saturation properties. The $P_{1/2}$ at 5 K was estimated to 7−8 mW, which is close to the value reported for the split S_3 signal earlier (*17*).

DISCUSSION

Interpretation of the Formation Spectra of the Split and Multiline EPR Signals. We have investigated the wavelength dependent induction of EPR signals from different states of the WOC. In the majority of studies involving the split EPR signals, broad spectrum light either in the visible or the NIR range has been used. In the present study, we have instead applied laser light with a narrow bandwidth to examine the wavelength dependence of the split signal inducing light for each of the split S_1, split S_3, split S_0, and S_2 multiline signals. The spin coupled signals were induced at 5 K in the S_1, S_3, and S_0 states while the S_2-state multiline EPR signal was induced at 0 °C by illumination in the visible and NIR regions. This difference in temperature is important since, in order to achieve reasonable spectra, the EPR sample must be very dense, which leads to difficulties in saturating the entire sample volume with a single or even multiple flashes. This problem is further enhanced by the freezing of the PSII enriched membranes, which then become opaque in the frozen state.[3] In our study these effects could not be avoided, and it is therefore not likely that our spectra reflect the true spectra of the light absorbing species. Instead the spectra reflect how efficiently the different EPR active species were induced at respective wavelength and temperature. We have therefore termed our spectra as "formation spectra" of the respective EPR signals.

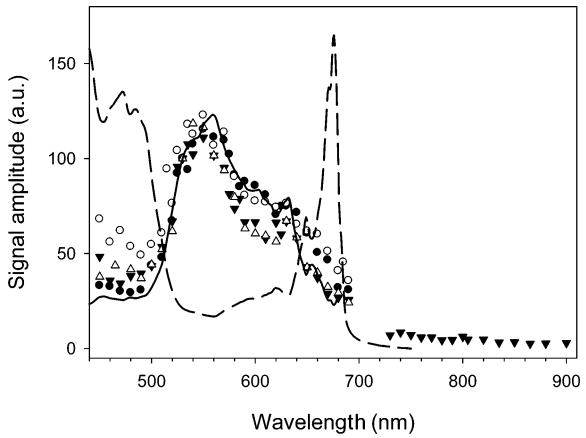

FIGURE 7: Comparison of the photon energy corrected formation spectra of the split S_0 (●), S_1 (○), and S_3 (▼) EPR signals and the S_2-state multiline EPR signal (△). The figure also shows the optical absorption spectrum of our PSII membranes at 1.7 K (dashed line) and its reciprocal (solid line). The formation spectra are from Figures 2D, 4B, and 5C and have been normalized to the photon content in the applied light (i.e., the applied flash energy divided by the energy of a single photon at a particular wavelength) at different wavelengths to reflect the absorption of the same number of photons. In addition, the photon energy corrected spectra were normalized at 530 nm to facilitate comparison of their spectral shapes.

Photon energy corrected formation spectra of these EPR signals, (i.e., spectra from Figures 2D, 4B, and 5C corrected for the applied number of photons at different wavelengths) are shown in Figure 7. Although not identical, all these formation spectra have important, similar features in the visible range. Some of these features fit well with the reciprocal of the PSII absorption spectrum obtained at liquid helium temperature (Figure 7). The maximum of the formation spectra is, in each case, observed around 550 nm where PSII shows its minimal absorption. Around 460 and 680 nm, where our PSII membranes have maximal absorption, the amplitudes in the formation spectra are about ∼25% of the maximum amplitude at 550 nm (Figure 7). Thus, the minimum at 550 nm in the PSII absorption is reflected in the most efficient induction of the EPR signals and vice versa, maxima in the PSII absorption give rise to minimum split and S_2 multiline signal formation.

For the concentrated EPR samples (>2 mg Chl/mL in our experiments) the penetration of the laser flash(es) is a problem and might significantly reduce the amount of PSII centers that can "see" light in the regions where the Chls absorb well. Our experiments using samples with reduced Chl concentrations did not solve this problem since the split signals became too small to allow spectral resolution of its formation. In contrast, penetration by green light is much more efficient and at 540 nm ∼60% of the

[3] Note that "glass-forming" agents such as high concentration of glycerol or ethylene glycol had to be avoided in our experiments as they interfere with the formation of the studied EPR signals.

PSII centers were excited with a single flash even with the quite weak flash from the MOPO (540 nm, 40 mJ). In a PSII membrane preparation there are about 200−250 Chl and 40−60 Car molecules per reaction center (*2*, *45*). This indicates that pigments other than Chls could be photoactive in this case and in the PSII core there are several Car molecules located in the vicinity of P_{680} (*2*, *13*, *15*). It is likely that this pool of Car molecules can both absorb and facilitate excitation energy transfer to P_{680}.

How can we explain the results in the visible region? It is agreed that the $S_1 \rightarrow S_2$ transition, and therefore the formation of the S_2-state multiline EPR signal, is a direct product of the charge separation in PSII. The formation spectrum of this signal, which was induced at optimal conditions at 0 °C, is rather similar to the formation spectra of the split signals, induced at 5 K (Figure 7). Thus, there is at first glance no reason to believe that the split signals originated from any other process in PSII than charge separation, at least in the visible light range. In the case of the split S_1 and split S_0 signals, which are not induced by NIR illumination, this conclusion is coherent with all data. Thus, the similarities between their formation spectra and the formation spectrum for the S_2 multiline signal (Figure 7) suggest that both the split S_1 and split S_0 signals are induced by normal photochemistry in PSII, involving photooxidation of Y_Z via P_{680}^+.

This is further supported by our earlier finding that both these signals decay almost completely in the minutes time scale at 5 K (*17*), probably by recombination with Q_A^- (*23*), which consequently was induced in all PSII centers giving rise to the split signals. By contrast, the split S_3 signal is induced, not only by visible light but also, and to what seems an even higher extent, by NIR illumination. In addition, in both cases when the signal is induced by visible light and when it is induced by NIR light, a large part of the spectrum is stable over prolonged time at 5 K (Figure 6A and ref *17*). This is discussed in the following section.

Interpretation of the Formation Spectrum of the Split S_3 Signal Induced by the Visible and NIR Illumination. It is agreed that the Mn_4Ca cluster undergoes oxidation during the $S_0 \rightarrow S_1$ and the $S_1 \rightarrow S_2$ state transitions. In contrast, the redox reaction involved in the $S_2 \rightarrow S_3$ transition is more controversial and it is debated whether this transition involves Mn-centered or ligand-centered oxidation (*46*, *47*). In either case, the properties of the S_3 state would be reflected in the formation spectrum and properties of the split S_3 EPR signal.

The split EPR signals are considered to reflect magnetic interaction between $Y_Z^\bullet$ and the Mn_4Ca cluster, the latter being different between the different S states. The spectral features, the maximally inducible signal amplitude, and the power saturation properties of the split S_3 signal induced by both visible and NIR illumination are similar (Figures 4 and 5). Therefore, we have no experimental reasons to believe that the magnetic configuration of the species involved in the split S_3 signal is different. In addition, we have now confirmed our previous result that it is possible to induce the split S_3 signal with visible light. Earlier this was carried out with broadband visible light (*17*, *24*) and in the present study this has been improved by the application of monochromatic laser light. This is in contrast to literature reports (*26*, *30*, *31*, *34*) that this signal can in fresh S_3 state samples only be induced by direct Mn-excitation using NIR light. Instead, our results leave little doubt that the split S_3 signal can be induced also by visible light in the entire wavelength region studied, 420−690 nm.

The induction of the split S_3 signal by NIR illumination does not involve normal PSII photochemistry, since P_{680} is not active above 730 nm (*48*). Therefore, alternative photochemistry is involved in the oxidation of Y_Z and formation of the EPR signal. Illumination with NIR light is known to induce low-temperature photochemistry in the Mn_4Ca cluster in the S_2 and S_3 states, including the formation of a split S_3 signal at 50 K. This is proposed to involve excitation of one of the Mn ions leading to alternative photochemistry in the WOC/Y_Z ensemble (*29*, *32*, *34*−*37*), and it has been proposed that the excited Mn ion is able to oxidize Y_Z directly to give $Y_Z^\bullet$, thereby giving rise to the split signal (*30*−*32*). The split S_3 signal we study here (induced at 5 K) is very similar to the split S_3 signal studied after induction at 50 K. It is thus likely that our studied formation of the split S_3 signal at 5 K involves a similar process. The NIR part of the formation spectrum of the split S_3 signal reported here for the signal induced at 5 K (Figure 5C, Figure 7) differs somewhat from a similar formation spectrum obtained for the split S_3 signal induced at 50 K (*34*). We find the maximum induction at 740 nm compared to the reported maximum yield at 760 nm in ref *34*. In addition, the peak of the spectrum in ref *34* was broader than the peak of the formation spectrum reported here (Figure 5C). The reason for these variations in the shape of the formation spectrum is unclear but could reflect the difference in the temperature of signal induction or the different origins of the PSII used in the two studies (spinach in our work; *Thermosynechococcus elongatus* in ref *34*).

The split S_3 signal generated with visible light decayed partly over time and, similar to previous reports (*17*), this decay involved a major fraction of the PSII centers that showed the split S_3 signal (∼50%; Figure 5A). As discussed above, it is likely that this decay to a large extent involved recombination with Q_A^-. By contrast, the split S_3 signal induced by the NIR irradiation was stable over hours (Figure 6A). This is explained by redox states in PSII produced by the different illumination regimes. Where visible light is used, Q_A^- is formed as a product of charge separation irrespective of which donor to P_{680}^+ is involved. This allows recombination with $Y_Z^\bullet$ in the split radical, and thus the gradual decay of the split signal. By contrast, when PSII is excited by NIR irradiation, P_{680} driven charge separation does not occur and in this case no Q_A^- is produced. The $Y_Z^\bullet$ radical formed would therefore lack a recombination "partner", thereby giving rise to a stable split signal. This was observed in the present study (Figure 6A).

Further confirmation for this hypothesis can be found by comparing the spectral shapes of the EPR signals generated by visible and NIR irradiation (Figures 4A and 5B). When the split S_3 signal was formed by illumination in the visible part of the spectrum, the recorded EPR spectrum was a mix of the split S_3 signal and a Car radical (Figure 6B, see also ref *17*) from the Car/Chl/Cytochrome b_{559} pathway (*49*−*52*). This is different from the EPR spectrum obtained by excitation in the NIR where the secondary donor pathway involving Car is not involved. Instead, the result of the illumination was a "clean" split S_3 signal. This is thus in agreement with the proposal of a "secondary donor-free" mechanism involving direct Mn excitation being involved

in the formation of the split S_3 signal by NIR illumination.

An interesting question, of mechanistic and functional importance, is whether both charge separation involving formation of P_{680}^+ (with visible light) and photochemistry at the Mn_4Ca cluster (with illumination in the NIR) at 5 K can produce similar magnetic interacting species responsible for the split S_3 signal, or if formation of the split S_3 signal in both the visible and the NIR regions involves a similar mechanism. Experiments attempting to clarify this phenomenon and to address the mechanistic implications are underway.

ACKNOWLEDGMENT

The optical spectrum from PSII enriched membranes at 1.7 K was kindly provided by Prof. Elmars Krausz (ANU, Canberra, Australia). We acknowledge valuable discussions with Prof. Leif Hammarström (Uppsala University, Sweden).

REFERENCES

1. Barber, J. (2003) Photosystem II: the engine of life, *Q. Rev. Biophys. 36*, 71−89.
2. Nelson, N., and Yocum, C. F. (2006) Structure and function of photosystems I and II, *Annu. Rev. Plant Biol. 57*, 521−565.
3. Kok, B., Forbush, B., and McGloin, M. (1970) Cooperation of charges in photosynthetic oxygen evolution. I. A linear four step mechanism, *Photochem. Photobiol. 11*, 457−475.
4. Clausen, J., and Junge, W. (2004) Detection of an intermediate of photosynthetic water oxidation, *Nature 430*, 480−483.
5. Haumann, M., Liebisch, P., Muller, C., Barra, M., Grabolle, M., and Dau, H. (2005) Photosynthetic O_2 formation tracked by time-resolved X-ray experiments, *Science 310*, 1019−1021.
6. Tommos, C., and Babcock, G. T. (2000) Proton and hydrogen currents in photosynthetic water oxidation, *Biochim. Biophys. Acta 1458*, 199−219.
7. Rappaport, F., and Lavergne, J. (2001) Coupling of electron and proton transfer in the photosynthetic water oxidase, *Biochim. Biophys. Acta 1503*, 246−259.
8. Renger, G. (2004) Coupling of electron and proton transfer in oxidative water cleavage in photosynthesis, *Biochim. Biophys. Acta 1655*, 195−204.
9. Blankenship, R. E., Babcock, G. T., Warden, J. T., and Sauer, K. (1975) Observation of a new EPR transient in chloroplasts that may reflect the electron donor to photosystem II at room temperature, *FEBS Lett. 51*, 287−293.
10. Razeghifard, M. R., Klughammer, C., and Pace, R. J. (1997) Electron paramagnetic resonance kinetic studies of the S states in spinach thylakoids, *Biochemistry 36*, 86−92.
11. Zouni, A., Witt, H. T., Kern, J., Fromme, P., Krauss, N., Saenger, W., and Orth, P. (2001) Crystal structure of photosystem II from *Synechococcus elongatus* at 3.8 Å resolution, *Nature 409*, 739−743.
12. Kamiya, N., and Shen, J. R. (2003) Crystal structure of oxygen-evolving photosystem II from Thermosynechococcus vulcanus at 3.7-Å resolution, *Proc. Natl. Acad. Sci. U.S.A. 100*, 98−103.
13. Ferreira, K. N., Iverson, T. M., Maghlaoui, K., Barber, J., and Iwata, S. (2004) Architecture of the photosynthetic oxygen-evolving center, *Science 303*, 1831−1838.
14. Biesiadka, J., Loll, B., Kern, J., Irrgang, K. D., and Zouni, A. (2004) Crystal structure of cyanobacterial photosystem II at 3.2 Å resolution: a closer look at the Mn-cluster, *Phys. Chem. Chem. Phys. 6*, 4733−4736.
15. Loll, B., Kern, J., Saenger, W., Zouni, A., and Biesiadka, J. (2005) Towards complete cofactor arrangement in the 3.0 Å resolution structure of photosystem II, *Nature 438*, 1040−1044.
16. Petrouleas, V., Koulougliotis, D., and Ioannidis, N. (2005) Trapping of metalloradical intermediates of the S-states at liquid helium temperatures. Overview of the phenomenology and mechanistic implications, *Biochemistry 44*, 6723−6728.
17. Havelius, K. G. V., Su, J. H., Feyziyev, Y., Mamedov, F., and Styring, S. (2006) Spectral resolution of the split EPR signals induced by illumination at 5 K from the S_1-, S_3- and S_0-states in Photosystem II, *Biochemistry 45*, 9279−9290.
18. Gilchrist, M. L., Ball, J. A., Randall, D. W., and Britt, R. D. (1995) Proximity of the manganese cluster of photosystem II to the redox-active tyrosine Y_Z, *Proc. Natl. Acad. Sci. U.S.A. 92*, 9545−9549.
19. Peloquin, J. M., Campbell, K. A., and Britt, R. D. (1998) ^{55}Mn pulsed ENDOR demonstrates that the photosystem II "split" EPR signal arises from a magnetically-coupled mangano-tyrosyl complex, *J. Am. Chem. Soc. 120*, 6840−6841.
20. Nugent, J. H. A., Muhiuddin, I. P., and Evans, M. C. W. (2002) Electron transfer from the water oxidizing complex at cryogenic temperatures: The S_1 to S_2 step, *Biochemistry 41*, 4117−4126.
21. Zhang, C. X., and Styring, S. (2003) Formation of split electron paramagnetic resonance signals in photosystem II suggests that tyrosine$_Z$ can be photooxidized at 5 K in the S_0 and S_1 states of the oxygen-evolving complex, *Biochemistry 42*, 8066−8076.
22. Koulougliotis, D., Teutlolf, C., Sanakis, Y., Lubitz, W., and Petrouleas, V. (2004) The $S_1Y_Z^\bullet$ metalloradical intermediate in photosystem II: an X- and W-band EPR study, *Phys. Chem. Chem. Phys. 6*, 4859−4863.
23. Zhang, C. X., Boussac, A., and Rutherford, A. W. (2004) Low-temperature electron transfer in photosystem II: A tyrosyl radical and semiquinone charge pair, *Biochemistry 43*, 13787−13795.
24. Su, J. H., Havelius, K. G. V., Mamedov, F., Ho, F. M., and Styring, S. (2006) Split EPR signals from photosystem II are modified by methanol, reflecting S state-dependent binding and alterations in the magnetic coupling in the $CaMn_4$ cluster, *Biochemistry 45*, 7617−7627.
25. Nugent, J. H. A., Turconi, S., and Evans, M. C. W. (1997) EPR investigation of water oxidizing photosystem II: Detection of new EPR signals at cryogenic temperatures, *Biochemistry 36*, 7086−7096.
26. Ioannidis, N., and Petrouleas, V. (2002) Decay products of the S_3 state of the oxygen-evolving complex of photosystem II at cryogenic temperatures. Pathways to the formation of the $S = 7/2$ S_2 state configuration, *Biochemistry 41*, 9580−9588.
27. Ioannidis, N., Zahariou, G., and Petrouleas, V. (2006) Trapping of the S_2 to S_3 state intermediate of the oxygen-evolving complex of photosystem II, *Biochemistry 45*, 6252−6259.
28. Su, J. H., Sigfridsson, K. G. V., Feyziyev, Y., and Styring, S. (2005) Flash-number dependent oscillation of split EPR signals from OEC in PSII induced by illumination at 5 K. In *Photosynthesis: Aspects to Global Perspectives* (van der Est, A., and Bruce, D., Eds.) Alliance Communications Group, Lawrence, KS.
29. Boussac, A., Sugiura, M., Inoue, Y., and Rutherford, A. W. (2000) EPR study of the oxygen evolving complex in His-tagged photosystem II from the cyanobacterium *Synechococcus elongatus*, *Biochemistry 39*, 13788−13799.
30. Ioannidis, N., and Petrouleas, V. (2000) Electron paramagnetic resonance signals from the S_3 state of the oxygen-evolving complex. A broadened radical signal induced by low-temperature near-infrared light illumination, *Biochemistry 39*, 5246−5254.
31. Ioannidis, N., Nugent, J. H. A., and Petrouleas, V. (2002) Intermediates of the S_3 state of the oxygen evolving complex of photosystem II, *Biochemistry 41*, 9589−9600.
32. Koulougliotis, D., Shen, J. R., Ioannidis, N., and Petrouleas, V. (2003) Near-IR irradiation of the S_2 state of the water oxidizing complex of photosystem II at liquid helium temperatures produces the metalloradical intermediate attributed to S_1Y_Z, *Biochemistry 42*, 3045−3053.
33. Sugiura, M., Rappaport, F., Brettel, K., Noguchi, T., Rutherford, A. W., and Boussac, A. (2004) Site-directed mutagenesis of the *Thermosynechococcus elongatus* photosystem II: The O_2-evolving enzyme lacking the redox-active tyrosine D, *Biochemistry 43*, 13549−13563.
34. Boussac, A., Sugiura, M., Kirilovsky, D., and Rutherford, A. W. (2005) Near-infrared-induced transitions in the manganese cluster of photosystem II: Action spectra for the S_2 and S_3 redox states, *Plant Cell Physiol. 46*, 837−842.
35. Boussac, A., Girerd, J. J., and Rutherford, A. W. (1996) Conversion of the spin state of the manganese complex in photosystem II induced by near-infrared light, *Biochemistry 35*, 6984−6989.
36. Boussac, A., Kuhl, H., Un, S., Rogner, M., and Rutherford, A. W. (1998) Effect of near-infrared light on the S_2-state of the manganese complex of photosystem II from Synechococcus elongates, *Biochemistry 37*, 8995−9000.
37. Baxter, R., Krausz, E., Wydrzynski, T., and Pace, R. J. (1999) Identification of the near-infrared absorption band from the Mn cluster of photosystem II, *J. Am. Chem. Soc. 121*, 9451−9452.
38. Berthold, D. A., Babcock, G. T., and Yocum, C. F. (1981) A highly resolved, oxygen-evolving photosystem-II preparation from spin-

ach thylakoid membranes: EPR and electron-transport properties, *FEBS Lett. 134*, 231−234.
39. Volker, M., Ono, T., Inoue, Y., and Renger, G. (1985) Effect of trypsin on PS-II particles. Correlation between Hill-activity, Mn-abundance and peptide pattern, *Biochim. Biophys. Acta 806*, 25−34.
40. Feyziyev, Y., van Rotterdam, B. J., Bernat, G., and Styring, S. (2003) Electron transfer from cytochrome b_{559} and $tyrosine_D$ to the S_2 and S_3 states of the water oxidizing complex in photosystem II, *Chem. Phys. 294*, 415−431.
41. Arnon, D. I. (1949) Copper enzymes in isolated chloroplasts. Polyphenoloxidase in beta-Vulgaris, *Plant Physiol. 24*, 1−15.
42. Styring, S., and Rutherford, A. W. (1988) Deactivation kinetics and temperature dependence of the S-state transitions in the oxygen-evolving system of Photosystem II measured by EPR spectroscopy, *Biochim. Biophys. Acta 933*, 378−387.
43. Styring, S., and Rutherford, A. W. (1987) In the oxygen-evolving complex of photosystem II the S_0 state is oxidized to the S_1 state by D^+ (Signal II_{slow}), *Biochemistry 26*, 2401−2405.
44. Sigfridsson, K. G. V., Su, J. H., Feyziyev, Y., and Styring, S. (2005) The spectral resolution of the "Split S_1" and "Split S_0" EPR-signals from photosystem II induced by illumination at 5 K. In *Photosynthesis: Aspects to Global Perspectives* (van der Est, A., and Bruce, D., Eds.) Alliance Communications Group, Lawrence, KS.
45. Wollman, F. A., Minai, L., and Nechushtai, R. (1999) The biogenesis and assembly of photosynthetic proteins in thylakoid membranes, *Biochim. Biophys. Acta 1411*, 21−85.
46. Messinger, J., Robblee, J. H., Bergmann, U., Fernandez, C., Glatzel, P., Visser, H., Cinco, R. H., McFarlane, K. L., Bellacchio, E., Pizarro, S. A., Cramer, S. T., Sauer, K., Klein, M. P., and Yachandra, V. K. (2001) Absence of Mn-centered oxidation in the $S_2 \rightarrow S_3$ transition: implication for the mechanism of water oxidation, *J. Am. Chem. Soc. 123*, 1804−7820.
47. Haumann, M., Muller, C., Liebisch, P., Iuzzolino, L., Dittmer, J., Grabolle, M., Neisius, T., Meyer-Klaucke, W., and Dau, H. (2005) Structural and oxidation state changes of the photosystem II manganese complex in four transitions of the water oxidation cycle ($S_0 \rightarrow S_1$, $S_1 \rightarrow S_2$, $S_2 \rightarrow S_3$, and $S_{3,4} \rightarrow S_0$) characterized by X-ray absorption spectroscopy at 20 K and room temperature, *Biochemistry 44*, 1894−1908.
48. Hughes, J. L., Smith, P., Pace, R. J., and Krausz, E. (2006) Charge separation in photosystem II core complexes induced by 690−730 nm excitation at 1.7 K, *Biochim. Biophys. Acta 1757*, 841−851.
49. Hanley, J., Deligiannakis, Y., Pascal, A., Faller, P., and Rutherford, A. W. (1999) Carotenoid oxidation in photosystem II, *Biochemistry 38*, 8189−8195.
50. Faller, P., Pascal, A., and Rutherford, A. W. (2001) Beta-carotene redox reactions in photosystem II: electron transfer pathway, *Biochemistry 40*, 6431−6440.
51. Tracewell, C. A., Cua, A., Stewart, D. H., Bocian, D. F., and Brudvig, G. W. (2001) Characterization of carotenoid and chlorophyll photooxidation in photosystem II, *Biochemistry 40*, 193−203.
52. Bautista, J. A., Tracewell, C. A., Schlodder, E., Cunningham, F. X., Brudvig, G. W., and Diner, B. A. (2005) Construction and characterization of genetically modified Synechocystis sp. PCC 6803 photosystem II core complexes containing carotenoids with shorter pi-conjugation than beta-carotene, *J. Biol. Chem. 280*, 38839−38850.

BI7004174